

X-Ray Properties of Early Type Galaxies as Observed with *ASCA*

H. Matsumoto¹, K. Koyama, H. Awaki, and T. Tsuru

Department of Physics, Kyoto University, Sakyo-ku, Kyoto, Japan 606-01

M. Loewenstein

Laboratory for High Energy Astrophysics, NASA/GSFC, Code 662, Greenbelt, MD 20771

and

K. Matsushita

Department of Physics, University of Tokyo, 7-3-1 Hongo, Bunkyo-ku, Tokyo, Japan 113

ABSTRACT

We have systematically investigated the *ASCA* spectra of 12 early type galaxies. This paper presents the global spectral properties of these systems based on a larger sample than in any previous *ASCA* study. The X-ray spectra were uniformly fitted by a two-component model consisting of hard X-rays from thermal emission with a temperature of about 10 keV or from a power-law with index 1.8, plus soft X-rays from a thin thermal plasma with temperature ranging from 0.3 to 1 keV. The X-ray luminosities of the hard component are found to be proportional to the blue band luminosities, while those of the soft component show large scatter with no clear correlation. The metal abundances determined from the soft component are systematically lower than solar, with a mean value of about 0.3 solar. We examine the relationships between the temperature and volume emission measure, and between the gas temperature and the stellar velocity dispersion. The volume emission measures for early type galaxies plotted as a function of the gas temperature are well below the extrapolated line found in clusters of galaxies, indicating that early type galaxies are relatively gas poor compared with galaxy clusters. The ratio of the stellar kinetic energy per unit mass to the thermal energy of the hot gas per unit mass (β_{spec}) is less than unity. We found no systematic relationship between X-ray properties and environment, suggesting that the interaction between interstellar matter and the intracluster medium is not strong.

Subject headings: galaxies: elliptical and lenticular, cD — X-rays: galaxies — X-rays: ISM

¹E-mail address: matumoto@cr.scphys.kyoto-u.ac.jp

1. Introduction

The *Einstein* satellite discovered X-ray emitting gas halos around luminous early type galaxies (eg. Forman, Jones, & Tucker 1985), forcing the rejection of previous assumptions that elliptical galaxies are gas poor systems. The X-ray surface brightness distribution was found to closely follow the optical image (Trinchieri, Fabbiano, & Canizares 1986); however the X-ray luminosity, and hence the mass of the hot gas, showed large scatter from galaxy to galaxy (eg. Canizares, Fabbiano, & Trinchieri 1987). The estimated cooling time of the hot gas is less than the Hubble time (Trinchieri et al. 1986), however cooling may be balanced by heating mechanisms such as supernova explosions. Arnaud et al. (1992) found that the iron mass in the intracluster medium (ICM) is directly proportional to the optical luminosity from early type galaxies in clusters of galaxies. This leads one to suspect that metals in the ICM originate in early type galaxies and that there might be a link, in the form of early star formation and galactic winds, between the ICM and metal abundances in early type galaxies. Due to the poor energy resolution of previous satellites, however, critical parameters for investigating the nature of the hot gas in early type galaxies, such as the gas temperature, mass, and metal abundance have not been well-constrained. Accordingly, several important issues including the origin, heating, and fate of the hot gas, and the effect of early type galaxies on the ICM, are not well understood.

ASCA (Tanaka et al. 1994) is the first satellite with sufficient energy resolution and large effective area over the broad 0.4 to 10 keV bandpass to determine these physical parameters. With this satellite, Awaki et al. (1994) analyzed 3 early type galaxies and found that the temperature and metal abundance of the hot gas are about 0.8 keV and 0.4 solar, respectively. The inferred metal abundance is lower than expected from theoretical models, and lower than those determined at other wavelengths. Accordingly, the *ASCA* observations raise a serious challenge to standard models for the evolution of galaxies and clusters of galaxies. This mystery deepened with the discovery of even lower metallicities (less than 0.2 solar) in two other elliptical galaxies (Loewenstein et al. 1994), and in the outer regions of NGC4636 (Mushotzky et al. 1994). Matsushita et al. (1994) discovered, analyzing 5 early type galaxies including the sample of 3 in Awaki et al. (1994), a hard X-ray component at energies above a few keV in addition to the hot gas component dominating below about 2 keV. In order to perform plasma diagnostics of the hot gas component, it is essentially important to estimate and remove the hard component from the X-ray spectra of early type galaxies. If the hard component is due to the integrated emission of stellar sources, as suggested by Matsushita et al. (1994), its luminosity should be proportional to optical luminosity. Since the samples in previous *ASCA* studies are too limited to fully investigate all the issues mentioned above, we have systematically studied twelve early type galaxies, including the samples of Awaki et al. (1994) and Matsushita et al. (1994) as well as newly observed galaxies. These comprise the largest sample of *ASCA* spectra of early type galaxies yet investigated.

2. Observations and Data Reduction

The galaxies we have selected for this study are NGC4472, NGC4406, NGC4636, NGC4649, NGC499, NGC507, NGC720, NGC4374, IC4296, NGC4382, IC1459 and NGC4365, which are listed in Table 1 with their optical parameters. The sample, which includes 7 performance and verification (PV) phase targets and 3 first-round guest investigator observations by the first author (HM), was principally selected on the basis of soft X-ray fluxes measured with the *Einstein* satellite in order to obtain useful spectra in reasonable exposure times. In addition to this criterion, a number of low X-ray luminosity galaxies were intentionally selected in order to detect and study possible differences between gas-rich and gas-poor galaxies. Furthermore, we selected our sample to include both galaxies in dense and tenuous gaseous environments in order to be able to study possible interaction between the ICM and interstellar medium (ISM).

All the galaxies were observed with two solid-state imaging spectrometers (SIS0 and SIS1) and two gas imaging spectrometers (GIS2 and GIS3) at the foci of 4 thin-foil X-ray mirrors (XRT) on board the *ASCA* satellite. Details of the instruments can be found in Burke et al. (1991), Ohashi et al. (1996a), Makishima et al. (1996), and Serlemitsos et al. (1995), while a general description of *ASCA* can be found in Tanaka et al. (1994). In table 2, we summarize the *ASCA* observation log of our sample galaxies. The data were screened with the standard selection criteria: data affected by the South Atlantic Anomaly, Earth occultation, and regions of low geomagnetic rigidity were excluded. We also eliminated contamination by the bright Earth, removed hot and flickering pixels for the SIS data, and applied rise-time rejection to exclude particle events for the GIS data. After the above data screening, we extracted X-ray spectra from circular regions centered on each galaxy with a uniform physical extraction radius of 38 kpc – the largest radius completely contained within the SIS field-of-view for all galaxies. The background spectra were obtained from source free regions around each galaxy.

3. Spectral Analysis and Results

In order to utilize the χ^2 technique, we rebinned the X-ray spectra to contain at least 20 counts in each spectral bin, then simultaneously fitted the spectra from the SIS0, SIS1, GIS2 and GIS3, with a common normalization factor but separate response functions for each detector, using the XSPEC (version 8.50) spectral fitting package.

Awaki et al. (1994) reported that the SIS spectra of bright early type galaxies, NGC4636, NGC4472 and NGC4406 exhibit emission lines from highly ionized Fe, Si, and S atoms. We further confirmed the presence of these emission lines in the spectra of the additional bright galaxies NGC4649, NGC499, NGC507 and NGC4374. Therefore we inferred that thin hot plasma emission is prevalent in bright early type galaxies and, hence, attempted to fit the X-ray spectra with a single temperature thermal plasma model (Raymond & Smith 1977; hereafter RS model) modified by interstellar absorption. The free parameters were the plasma temperature, metal

abundance, photoelectric absorption column density, and normalization. The abundances are collectively varied keeping the relative ratio at the solar value (Anders & Grevesse 1989).

This model, however, failed to reproduce the observed spectra except that of NGC499. From all galaxies, systematic excess emission is found above the 4 keV band. A typical example, NGC4649, is shown in figure 1. Thus we found the presence of hard X-ray emission, as previously reported in several individual galaxies (Kim, Fabbiano & Trinchieri 1992; Matsushita et al. 1994), to be a ubiquitous property of elliptical galaxies. In figure 2 we compare the X-ray spectra of the two elliptical galaxies NGC4636 and NGC4365; although they have nearly identical optical blue luminosities, the former is X-ray bright and the latter is X-ray faint. The difference in X-ray flux is confined to the soft X-ray band: the X-ray spectrum of NGC4636 below 3 keV is nearly two orders of magnitude brighter than that of NGC4365. On the other hand, the X-ray spectra above the 4keV band are indistinguishable, as might be expected based on the identical optical blue band magnitudes. Thus we compared the X-ray spectra above the 4 keV band for the entire sample, and found no evidence of significant differences in spectral shape, although the absolute fluxes vary from galaxy to galaxy. Accordingly, we assumed a thermal bremsstrahlung model for the hard component to estimate the temperature variation using the data above 4 keV. Since the statistics are limited, however, we could only determine a lower limit on the temperature of the bremsstrahlung model of about 2 keV. Since the GIS has higher sensitivity than the SIS in the relevant high energy band, we co-added all of the GIS spectra in our sample to improve the statistical accuracy. Figure 3 shows the composite GIS 2 and 3 spectra above the 4 keV band. We fitted a thermal bremsstrahlung model to this spectrum, and obtained an acceptable fit ($\chi^2/d.o.f.$ of 22.36/31) with the best-fit temperature $12.0^{+29.3}_{-5.5}$ keV (hereafter, errors are 90 % confidence unless otherwise stated). This composite spectrum is equally well fitted ($\chi^2/d.o.f.$ of 22.83/31) by a power law model with photon index 1.8 ± 0.4 . Therefore, we cannot distinguish between the two possible origins – thermal and non-thermal – of the hard component from the spectrum alone. However the relevant physical parameters, such as the X-ray luminosity (L_X) of the hard component, or iron K-shell line flux do not significantly differ whether we use thermal bremsstrahlung or power-law models. Thus we assume the thermal-bremsstrahlung model for further discussion.

In order to estimate the strength of Fe K line emission, we added a Gaussian line to the above model. The best-fit temperature is slightly altered to $8.8^{+13.9}_{-3.7}$ keV, with line center energy and equivalent width of the Gaussian of $6.4^{+0.3}_{-0.4}$ keV and $220(< 460)$ eV, respectively. Confidence contours of the line energy and equivalent width at $\Delta\chi^2 = 2.71, 4.61$ and 9.21 are plotted in Figure 4. Adding the line decreased χ^2 from 22.36 to 18.50, which is not statistically significant (Malina, Lampton & Bowyer 1976). Therefore we can conclude that the composite hard component spectrum requires no significant emission lines.

Since the presence of both emission lines from highly ionized heavy elements in the low energy band and a hard X-ray tail at the high energy band seem to be common in the galaxies in our sample, we fitted two-component models to all broad band spectra. The models consist of

a thermal bremsstrahlung component with a fixed temperature of 12 keV determined from the composite hard band spectrum, plus a thin thermal model (RS model) for the soft band emission. The column density of the hard component was constrained to be the same as that of the RS model. The free parameters were the temperature and metal abundance of the RS model, the column density, and normalizations for both the RS and bremsstrahlung models. The best-fit parameters and 90% confidence errors are listed in Table 3. We generally found reasonable fits with this unified model, however two galaxies – NGC4636 and NGC507 – exhibit unacceptably large values of χ^2 . Although these two galaxies may require more complicated modeling (NGC4636 was found to have both an abundance gradient and an extra centrally concentrated cool component by Mushotzky et al. 1994), more detailed study of individual galaxies is beyond the scope of this paper. The best-fit RS abundances and temperatures are in excellent agreement with those derived from *ROSAT* PSPC observations (Davis & White 1996; Kim & Fabbiano 1995), except for NGC4472 where the *ASCA* parameters are consistent only with the central PSPC parameters (Forman et al. 1993). Significant excess absorption is required by the *ASCA*, but not the PSPC, spectra of NGC4472, NGC4406, and NGC4649. This discrepancy is likely due either to remaining inaccuracies in the *ASCA* low energy response, or to the inadequacy of the simple foreground screen model that we employ for the absorption.

Many authors have pointed out systematic differences in the best-fit parameters between models using different plasma emission codes. We thus examined this possible systematic and model-dependent uncertainty by comparing the RS and MEKA models (Mewe, R., Gronenschild, E.H.B.M., and van den Oord, G.H.J. 1985). In figures 5a – d, we show the correlation plots of best-fit parameters between the RS and MEKA models: the column density (a), temperature (b), metal abundance (c), and X-ray luminosity (d). The best-fit column densities are found to be consistent within the errors, while best-fit temperatures in the MEKA model are almost 20 % lower than the RS model. The metal abundances in the MEKA model generally have larger values than the RS model, although the scatter in the correlation plot is large. As for the luminosity, both models give essentially the same best-fit value. Thus we confirmed the existence of plasma model-dependent systematic and non-systematic errors. However these do not largely effect the following discussion, hence we refer to the best-fit values using the RS model.

4. Discussion

4.1. The Hard Component

Figure 6 shows the relation between the X-ray luminosity (L_X) of the hard component in the 0.5–4.5 keV band and the blue band luminosity (L_B). The uncertainties in L_X of the hard component are typically $\sim 30\%$. The solid line is the best-fit relation between the blue luminosity and the 0.5–4.5 keV band luminosity found for bulge-dominated spiral galaxies (Canizares et al. 1987). We found that L_X of the hard component is proportional to L_B , and that the constant

of proportionality is nearly the same as found in spiral galaxies: L_X/L_B for the hard component in early type galaxies is generally consistent with that of bulge-dominated spiral galaxies like M31. The excess hard flux in the radio galaxies IC1459 and IC4296 probably can be explained by X-ray emission from AGN; indeed our analysis of archival PSPC data from IC1459 indicates the presence of an unresolved hard component. Furthermore, we found that the composite *ASCA* GIS spectrum above the 4keV band (Section 3) resembles the X-ray spectra of bulge-dominated spiral galaxies which can be fitted with a thermal bremsstrahlung model with $kT \gtrsim 5$ keV (eg. Makishima et al. 1989).

These facts suggest that early type galaxies contain a hard X-ray component attributable to the same origin as X-rays in bulge-dominated spiral galaxies. Since the X-ray emission from bulge-dominated spirals is thought to arise from a population of low-mass X-ray binaries (LMXB), we suspect that the primary hard component in early type galaxies is also due to the integrated emission of an ensemble of LMXB. Matsushita et al. (1994) came to the same conclusion based on a more limited (5 galaxies) sample; they also discovered that the hard component is generally extended which argues against an AGN power-law origin for the hard component. With a larger galaxy sample than Matsushita et al. (1994), we therefore confirm that both the shape and relative magnitude of the hard component in early type galaxies is consistent with that in bulge-dominated spiral galaxies, strengthening the suggestion that the hard X-ray component in early type galaxies is due to LMXB.

Although LMXB usually exhibit a weak 6.7 keV iron line, we found no significant iron line in the early type galaxies. The 90 % confidence upper limit on the equivalent width of the Fe $K\alpha$ line of 500 eV is too large to place any strong constraints on the LMXB scenario.

4.2. The Soft Component

Emission lines from highly ionized Fe, Si, and S are detected from the 7 galaxies in our sample with the best statistics; non-detection of emission lines for the other galaxies is consistent with their having a lower signal-to-noise ratio. The existence of these emission lines is direct evidence for the prevalence of thin hot interstellar plasma in bright early type galaxies. We now discuss the nature of this plasma using our results, as well as referring to published optical data.

4.2.1. Correlation between kT and VEM

Because L_X of the hard component is generally proportional to L_B , the large dispersion in the total L_X - L_B diagram (Canizares et al. 1987) is mainly due to a spread in L_X of the soft component. This is illustrated in figure 7 where L_X of the soft component is plotted versus L_B . Since, ignoring the mostly small variations in temperature, L_X of the soft component is

proportional to the volume emission measure (VEM), and

$$VEM \equiv \int n_e n_p dV \sim M_{gas}^2 / V$$

, where n_e and n_p are the densities of electrons and protons, respectively, and V and M_{gas} are, respectively, the volume and mass of the hot gas, the large dispersion in L_X found in figure 7 indicates the presence of a wide mass range of hot gas in early type galaxies.

Figure 8 is a plot of the volume emission measure (VEM) versus the temperature of the hot gas. For comparison, we show the data for clusters of galaxies in the same figure with plus symbols (Hatsukade 1989). The Spearman rank correlation coefficient between VEM and temperature for early type galaxies is estimated to be 0.43; therefore, we cannot conclude that there is a strong correlation between temperature and mass of the hot gas. The line in the figure shows the best-fit relation for the cluster data. What is clear is the fact that most of our galaxy sample is located well below the cluster correlation line, and that VEM drops steeply with kT from rich cluster all the way down to galaxy scales. Since for a constant gas mass as a fraction of gravitational mass $VEM \propto kT^{1.5}$, it is clear that early type galaxies are far more gas poor than clusters.

4.2.2. Heating Mechanism

Figure 9 presents the relation between the stellar velocity dispersion and the hot gas temperature. The velocity dispersions of the galaxies in clusters are shown with plus signs (Hatsukade 1989). The solid line represents $\beta_{spec} = 1$, where

$$\beta_{spec} \equiv \frac{\mu m_H \sigma^2}{kT}$$

, and μ , m_H , σ , k and T are mean molecular weight (we assumed it to be 0.6), proton mass, stellar (or galaxy) velocity dispersion, Boltzmann constant, and temperature, respectively. $\beta_{spec} = 1$ indicates that the thermal energy of the hot gas per unit mass is equal to the stellar (or galactic) kinetic energy per unit mass. The Spearman rank correlation coefficient for early type galaxies between σ and temperature is estimated to be 0.54, which is not significant. Thus we cannot strongly conclude that there is a positive correlation between these two parameters which would indicate a correlation between the depth of the gravitational potential and the temperature of the hot gas as expected for equilibrium systems. However, all our sample galaxies show higher temperatures than would be expected based on the best-fit cluster sample correlation line; *i.e.* β_{spec} is less than 1 for all of the early type galaxies in our sample compared to approximately 1 for clusters of galaxies. In other words, the thermal energy of the hot gas per unit mass is larger than the stellar kinetic energy per unit mass.

Figure 10 shows the relation between the velocity dispersion and β_{spec} . The mean value of β_{spec} , weighted using relative errors, is about 0.5. If the stars and gas in early type galaxies are

both isothermal and in hydrostatic equilibrium, $\rho_{gas} \propto \rho_{gal}^{\beta_{spec}}$, where ρ_{gas} and ρ_{gal} are the densities of hot gas and stars in the galaxy, respectively (eg. Sarazin 1986). Trinchieri et al. (1986) have found that for bright early type galaxies, the X-ray and optical surface brightness tend to follow each other. Since the X-ray brightness profile traces ρ_{gas}^2 and the optical profile traces ρ_{gal} , this implies that β_{spec} is about 0.5 (Fabbiano 1989), consistent with our direct measurement of β_{spec} . $\beta_{spec} = 0.5$ is expected if cooling (proportional to ρ_{gas}^2) is approximately balanced by heating by stellar winds, gravitational compression in an inflow, or Type Ia supernovae that all scale as the local stellar density.

Assuming that the present-day stellar mass loss rate is about $1.5 \times 10^{-11} L_B M_\odot / yr$ and has decreased with time as $t^{-1.3}$ (Ciotti et al. 1991), we see that the typical mass of hot gas observed in early type galaxies ($10^{9-10} M_\odot$) is much less than the total accumulated over the Hubble time ($\sim 10^{11} M_\odot$). This fact in conjunction with $\beta_{spec} = 0.5$ and the short cooling times of the hot gas in the central regions ($\sim 10^6 - 10^8$ yr; Fabbiano 1989) implies that either (1) there is some heating mechanism that balances cooling and has driven much of the stellar mass loss out of the galaxy, or (2) an inflow is occurring where the primary heating mechanism is gravitational compression and where there must be some sink for gas cooling below X-ray emitting temperatures.

One may argue that a plausible heating mechanism is type Ia supernova explosions. We consider a simple model where the energy of supernova explosions is constant ($\sim 10^{51}$ erg) and the energy deposited per unit gas mass uniform over the entire galaxy. Let $k\Delta T$ be the “excess temperature” – the difference between the temperature of the hot gas and that corresponding to the stellar velocity dispersion,

$$k\Delta T \equiv kT_{hot\ gas} - \mu m_H \sigma^2.$$

Since we are considering emission from a standard volume, the mass of the hot gas is proportional to the square root of VEM (Section 4.1.1), and the supernova rate thought to be proportional to L_B . If heating by type Ia supernovae is important, we would expect a negative correlation between $k\Delta T$ and $VEM^{1/2}/L_B$ because the rise in gas temperature should be smaller as the gas mass per supernova becomes larger.

Figure 11 shows the plot of $VEM^{1/2}/L_B$ vs. $k\Delta T$. Since the Spearman rank correlation coefficient is 0.40, we can conclude that there is no negative correlation. This contradicts simple models where the heating source is proportional to L_B and the efficiency of heating is uniformly high, but rather suggests that the efficiency of energy transfer to the hot gas may increase as the gas mass per star becomes larger. A negative correlation between $VEM^{1/2}/L_B$ and Fe abundance would also be predicted by a simple SNIa-dominated heating model (see below), and is likewise not seen.

The importance of heating by type Ia supernovae can generally be ruled out on the basis of the observed constraints on the iron abundance, since each explosion injects $\sim 0.7 M_\odot$ of Fe into the hot gas. This means that increasing the gas temperature by ~ 0.5 keV will enhance the Fe abundance by ~ 1 in solar units. Even if we attribute all of the Fe in the hot gas to supernova

explosions – an extreme assumption considering the expected contribution from stellar mass loss (Section 4.2.3) – supernova heating cannot explain the observed values of $k\Delta T$ in most of our sample.

4.2.3. Metal Abundance

Figure 12 shows the relation between the abundance and the temperature. We can see no clear correlation between these parameters, although the lowest metallicities are found in the galaxies with the coolest ISM. If we use the MEKA model, these conclusions are not essentially altered.

For the galaxies whose metal abundances are well determined, the abundances, without exception, are found to be less than half solar. These values are considerably lower than theoretical expectations, and those determined at optical wavelengths. An abundance gradient (Mushotzky et al. 1994) may partially account for the discrepancy between optical abundances, which are determined in the central region of the galaxy, and X-ray abundances measured over a region extending to many effective radii.

Significantly sub-solar metallicities have also been observed with *ASCA* in a variety of sources, including stellar coronae (eg. Singh, Drake, & White 1995), starburst galaxies (eg. Awaki et al. 1995; Tsuru et al. 1996), and supernova remnants (SNRs) (eg. Hayashi et al. 1996). We think it is worth noting that some SNRs in the Large Magellanic Cloud sufficiently evolved to sweep up large amounts of ISM exhibit X-ray spectra which closely resemble those of early type galaxies (Hayashi et al. 1996). Improvements in our understanding of the processes of enrichment by supernovae and stellar mass loss may help solve the puzzle of low abundances if, for example, the gas ejected from supernovae does not mix well into the ISM and the gas which is overly dense and metal-rich cools and drops out of the X-ray emitting hot gas (Fujita, Fukumoto, & Okoshi 1996).

Arimoto et al. (1996) suggest that low abundances may be an artifact, since the metal abundance is constrained by Fe L emission lines around 1 keV for which the atomic physics parameters are poorly known. However, Hwang et al. (1996) have found that, for hot gas temperatures between 2 and 4 keV, the abundance determined from Fe L and Fe K lines is fairly consistent (with abundances determined from the Fe L region actually slightly higher), and any errors in the abundances due to atomic physics uncertainties that exist in the current codes are unlikely to exceed 30 – 50 %. Therefore plasma model uncertainties may not explain the low abundances, although the increasing complexity of Fe L emission for temperatures below 1 keV imply that more detailed analysis than lies within the scope of this paper is needed to solve this problem. We note that the consistency of Fe abundances derived independently over a wide range of ionization states in stellar coronae (eg. Drake 1996) and the comparably low abundances inferred for ions with more straightforward atomic parameters (eg. Si; Ohashi et al. 1996b) implies that it is unlikely that the abundances derived here are underestimated by large factors.

Weak constraints on oxygen abundances are available only for the 3-brightest early type galaxies (NGC4472, NGC4406, and NGC4636); other galaxies have insufficient signal-to-noise ratios. The best fit oxygen abundances for the 3 galaxies we derive are consistent with those found by Awaki et al. (1994), roughly equal to the iron abundances. The oxygen abundances are not determined to sufficient accuracy to place significant constraints on the relative contributions of SNII and SNIa to the heavy metal production in the observed galaxies.

4.2.4. Interaction between ISM and ICM

Our sample includes galaxies in both relatively dense and tenuous intergalactic environments. NGC4636, for example, is very far from the center of the Virgo cluster and no nearby ICM X-ray emission is seen, while NGC4472, the central galaxy of a subgroup in the Virgo cluster, is surrounded by significant ICM X-ray emission. NGC720, at the center of the poor group LGG38 (Garcia 1993), on the other hand, does not show effects from either ram pressure or tidal distortion, hence is regarded as rather isolated (Buote & Canizares 1996).

For all the correlations shown in figures 6 – 12, we see no systematic differences between the galaxies in dense and tenuous gaseous environments. This indicates that the interaction between the ICM and ISM is not strong enough to manifest itself in our sample. More comprehensive investigations of such interactions require detailed study of spatial variations in X-ray spectral properties as in Iwasawa et al. (1996) who have found evidence for ram pressure stripping of the ISM in NGC4406, as well as a larger sample spanning a wider range of environments.

5. Conclusion

We have presented results from the uniform analysis of the *ASCA* spectra of 12 early type galaxies. This is the largest such sample to date and, as summarized below, we have uncovered new facts as well as confirmed previous inferences based on much smaller samples.

1. We found that the X-ray spectra from the 12 galaxies in our sample generally consist of at least two components: a soft component from X-ray emission of hot gas, and a hard component that can be characterized by either a thermal bremsstrahlung model with $kT > 5$ keV or a power-law model of photon index 1.8. The consistency of the strength and spectral shape of the hard component with those in bulge-dominated spirals corroborates previous suggestions that it primarily originates as the integrated emission from X-ray binaries. The hard component spectrum requires no significant Fe K line emission, and the upper limit on the equivalent width of Fe K line emission is 460 eV.
2. We confirmed that the metal abundance of the hot gas is generally less than 0.5 solar. There is no clear correlation between the abundance and temperature of the hot gas, however the

lowest abundances are found in the coolest galaxies.

3. There is a large dispersion in the ratio of gas mass (*i.e.* the X-ray luminosity of the soft component) to optical luminosity, implying a wide variety of gas-dynamical histories.
4. Theories of large-scale structure imply that there is a continuum of dark matter halos spanning galaxy and cluster scales. However, we have found that early type galaxies fall well below the constant gas mass fraction extension of the hottest clusters in the $kT - VEM$ plane ($VEM \propto kT^{1.5}$), and that the ratio of thermal to kinetic energy per unit mass is, on average, twice that found for clusters of galaxies. This suggests that larger systems are generally more efficient at retaining their hot gas and less efficient at converting gas into stars. The interstellar media of elliptical galaxies are not simply scaled down version of intracluster media, but have been more profoundly effected by feedback from star formation and other gas-dynamical processes.
5. The low Fe abundances, as well as the absence of a negative correlation between the “excess temperature”, defined as the difference between the hot gas temperature and the temperature corresponding to the stellar velocity dispersion, and the ratio of the square root of the volume emission measure of the hot gas to the blue band luminosity (an indicator of the mass ratio of hot gas to stars) argue against type Ia supernovae being an important heat source for the ISM.
6. We found no systematic differences in the physical parameters of the hot gas between galaxies in dense and tenuous intracluster environments, although our ability to test this is limited. This indicates that interaction between the intracluster medium and interstellar matter may not be strong.

In short, *ASCA* analysis of early type galaxies has yielded both expected (a hard component with the same normalization as in spiral bulges) and unexpected (low interstellar abundances) results. The interrelationships and dispersion among the properties of the hot gas component, and their comparison with those in intracluster media demonstrates the relative importance of astration, mass loss, and gas-dynamics in determining the evolution of early type galaxies and their ISM. Any complete theory of galaxy formation must explain the observed trends and diversity of bound distributions of hot gas on galaxy and cluster scales.

We thank all of the members of the *ASCA* team and the launching staff of the Institute of Space and Astronautical Science.

REFERENCES

Anders, E., & Grevesse, N. 1989, *Geochim. Cosmochim. Acta*, 53, 197

- Arimoto, N., Matsushita, K., Ishimaru, Y., Ohashi, T., & Renzini, A. 1996, preprint
- Arnaud, M., Rothenflug, R., Boulade, O., Vigroux, L., & Vangioni-Flam, E. 1992, *A&A*, 254, 49
- Awaki, H. et al. 1994, *PASJ*, 46, L65
- Awaki, H., Tsuru, T., Koyama, K., & *ASCA* team 1996, in *UV and X-Ray Spectroscopy of Astrophysical and Laboratory Plasmas*, ed. Yamashita, K., and Watanabe, T. (Tokyo, Japan: Universal Academy Press, Inc.), 327
- Buote, D. A. & Canizares, C. R. 1996, *ApJ*, 468, 184
- Burke, B. E., Mountain, R. W., Harrison, D. C., Bautz, M. W., Doty, J. P., Ticker, G. R., & Daniels, P. J. 1991, *IEEE Trans. ED-38*, 1069
- Canizares, C. R., Fabbiano, G., & Trinchieri, G. 1987, *ApJ*, 312, 503
- Ciotti, L., D’Ercole, A., Pellegrini, S., & Renzini, A., 1991 *ApJ*, 376, 380
- Davis, D. S., & White, R. E. III, 1996, *ApJ*, in press
- de Vaucouleurs, G., de Vaucouleurs, A., Corwin, Jr., H. G., Buta, R. J., Paturel, G., & Fouqué, P. 1991, *Third Reference Catalogue of Bright Galaxies* (New York: Springer-Verlag) (RC3)
- Donnelly, R. H., Faber, S. M., & O’Connell, R. M. 1990, *ApJ*, 354, 52
- Drake, S. A. 1996, in *Cosmic Abundances*, ed. Holt, S. S., and Sonneborn, G. (Astronomical Society of the Pacific Press)
- Fabbiano, G. 1989, *ARA&A*, 27, 87
- Forman, J. C., Jones, C., David, L., Franx, M., Makishima, K., & Ohashi, T. 1993, *ApJ*, 418, L55
- Forman, J. C., Jones, C., & Tucker, W. 1985, *ApJ*, 293, 102
- Fujita, Y., Fukumoto, J., & Okoshi, K. 1996, *ApJ*, in press
- Garcia, A. M. 1993, *A&AS*, 100, 47
- Hatsukade, I. 1989, PhD. thesis, Osaka University
- Hayashi, I. et al., 1996, in preparation
- Huchra, J. P., & Geller, M. J., 1982, *ApJ*, 257, 423
- Hwang, U., Mushotzky, R. F., Loewenstein, M., Markert, T. H., Fukazawa, Y., & Matsumoto, H. 1996, *ApJ*, in press
- Iwasawa, K., White, D. A., & Fabian, A. C. 1996, *MNRAS*, submitted
- Kim, D. -W., Fabbiano, G., & Trinchieri, G., 1992, *ApJ*, 393, 134
- Kim, D. -W., & Fabbiano, G. 1995, *ApJ*, 441, 182
- McElroy, D. B. 1995, *ApJS*, 100, 105
- Loewenstein, M., Mushotzky, R. F., Tamura, T., Ikebe, Y., Makishima, K., Matsushita, K., Awaki, H., & Serlemitsos, P. J. 1994, *ApJ*, 436, L75

- Makishima, K. et al. 1989, PASJ, 41, 697
- Makishima, K. et al. 1996, PASJ, 48, 171
- Malina, R., Lampton, M., & Bowyer, S., 1976, ApJ, 209, 678
- Matsushita, K. et al., 1994, ApJ, 436, L41
- Mewe, R., Gronenschild, E. H. B. M., & van den Oord, G. H. J. 1985, A&AS, 62, 197
- Mushotzky, R. F., Loewenstein, M., Awaki, H., Makishima, K., Matsushita, K., & Matsumoto, H., 1994, ApJ, 436, L79
- Ohashi, T. et al. 1996a, PASJ, 48, 157
- Ohashi, T. et al. 1996b, in UV and X-ray Spectroscopy of Astrophysical and Laboratory Plasmas, ed. Yamashita, K., and Watanabe, T. (Tokyo, Japan: Universal Academy Press, Inc.), 151
- Raymond, J. C., & Smith, B. W. 1977, ApJS, 35, 419
- Sarazin, C. L. 1986, Rev. Mod. Phys., 58, 1
- Serlemitsos, P. J. et al. 1995, PASJ, 47, 105
- Singh, K. P., Drake, S. A., & White, N. E. 1995, ApJ, 445, 840
- Stark, A. A., Gammie, C. F., Wilson, R. W., Bally, J., Linke, R. A., Heiles, C., & Hurwitz, M. 1992, ApJS, 79, 77
- Tanaka, Y., Inoue, H., & Holt, S. S. 1994, PASJ, 46, L37
- Tonry, J. L., and Davis, M., 1981, ApJ, **246**, 666.
- Trinchieri, G., Fabbiano, G., & Canizares, C. R. 1986, ApJ, 310, 637
- Tsuru, T. et al. 1996, PASJ, submitted

Fig. 1.— An example (NGC4649) of the single-temperature model fitting. Only the data for the SIS0 and GIS2 are shown. The solid lines show the best-fit single-temperature model.

Fig. 2.— The SIS0 spectra of NGC4636 (filled circles) and NGC4365 (open circles).

Fig. 3.— The composite GIS spectra of our targets above the 4 keV band. The solid line shows the best-fitting thermal bremsstrahlung model.

Fig. 4.— Confidence contours at $\Delta\chi^2 = 2.71, 4.61$ and 9.21 for the line center energy and equivalent width of the Fe-K line.

Fig. 5.— The relation between the best-fit parameters of the RS and MEKA models: (a) the column density, (b) the plasma temperature, (c) the metal abundance, (d) L_X of the soft component. In these figures, galaxies whose parameters were not well constrained are not shown.

Fig. 6.— The X-ray luminosity of the hard component vs. the blue band luminosity. The downward arrow shows upper limit of NGC499. The line shows the relation for spiral galaxies (Canizares, Fabbiano, & Trinchieri 1987).

Fig. 7.— The X-ray luminosity of the soft component vs. the blue band luminosity. The line is the same as shown in Figure 6.

Fig. 8.— The volume emission measure vs temperature of the hot gas. Plus symbols denote clusters of galaxies. The line shows the best fit relation for the cluster data.

Fig. 9.— The velocity dispersion vs. the gas temperature. The solid line is given by the equation $\beta = \mu m_H \sigma^2 / kT = 1$. The symbols are the same as in Figure 8.

Fig. 10.— The stellar velocity dispersion vs. β_{spec} .

Fig. 11.— The ratio of the square root of the X-ray luminosity of the hot gas to the blue band luminosity vs. $k\Delta T$, where $\Delta T = T_1 - T_2$, T_1 is the gas temperature, and T_2 is the temperature predicted from the velocity dispersion assuming $\beta = \mu m_H \sigma^2 / kT_2 = 1$.

Fig. 12.— The metal abundance vs. the hot gas temperature.

Table 1. Target data

Name	RA ^a (2000)	DEC ^a (2000)	Distance ^b (Mpc)	B_0^T ^c (mag)	M_B ^d (mag)	$\log\left(\frac{L_B}{L_\odot}\right)$ ^e	Type ^f	σ ^g (km/sec)	N_H ^h (cm^{-2})	Group ⁱ
NGC4472(M49)	12 29 46.5	07 59 58	25.8	9.26	-22.80	11.28	E2	315	1.6e20	Virgo
NGC4406(M86)	12 26 11.8	12 56 49	25.8	9.71	-22.35	11.10	E3	256	2.7e20	Virgo
NGC4636	12 42 49.8	02 41 17	25.8	10.37	-21.69	10.84	E0-1	217	1.9e20	Virgo
NGC4649(M60)	12 43 40.3	11 32 58	25.8	9.70	-22.36	11.11	E2	344	2.4e20	Virgo
NGC499	01 23 11.6	33 27 36	94.5	12.79	-22.09	11.00	S0 ⁻	235	5.3e20	Pisces
NGC507	01 23 40.1	33 15 22	94.5	12.19	-22.69	11.24	SA(r)0 ⁰	306	5.3e20	Pisces
NGC720	01 53 00.4	-13 44 21	39.6	11.13	-21.86	10.91	E5	224	1.4e20	LGG38
NGC4374(M84)	12 25 03.7	12 53 15	25.8	9.91	-22.15	11.02	E1	296	2.6e20	Virgo
IC4296	13 36 38.9	-33 57 59	72.8	11.42	-22.89	11.32	E	290	4.3e20	HG22
NGC4382(M85)	12 25 24.7	18 11 27	25.8	9.95	-22.11	11.01	SA(s)0 ⁺ _{pec}	200	2.7e20	Virgo
IC1459	22 57 10	-36 27 42	43.0	10.83	-22.34	11.10	E3-4	316	1.2e20	HG15
NGC4365	12 24 27.9	07 19 06	25.8	10.42	-21.64	10.82	E3	262	1.6e20	Virgo

^a2000 epoch coordinates from the Third Reference Catalogue of Bright Galaxies; de Vaucouleurs et al. 1991, hereafter RC3

^bDistance from Donnelly, Faber, & O’Connell 1990. For NGC499 and NGC507, we adopt the distance from Kim & Fabbiano 1995

^c B magnitude, where we list B_0^T from RC3

^dAbsolute blue magnitude calculated with the distances in the 4th column

^eBlue band luminosity in solar units, defined as $\log L_B = -0.4(M_B - 5.41)$

^fMorphological type from RC3

^gStellar velocity dispersion from Canizares, Fabbiano & Trinchieri 1987, Tonry & Davis 1981, and McElroy 1995

^hGalactic column density from Stark et al. 1992

ⁱName of group to which the galaxy belongs. “Virgo” denotes the Virgo cluster of the galaxies, “Pisces” denotes the Pisces group, “LGG” denotes a group in Garcia 1993, and “HG” denotes a group in Huchra & Geller 1982

Table 2. *ASCA* observation log

Target	Date (yy/mm/dd)	Radius (arcmin)	SIS mode ^a		Exposure (ksec)				count rate ^b (ksec)			
					SIS0	SIS1	GIS2	GIS3	SIS0	SIS1	GIS2	GIS3
NGC4472	1993/07/04	5	B	4	20.1	20.1	21.5	21.5	0.39	0.31	0.13	0.16
NGC4406	1993/07/03	5	F	4/2	19.7	19.7	20.8	20.8	0.34	0.27	0.11	0.13
NGC4636	1993/06/22	5	B	4	38.3	38.4	37.6	37.6	0.38	0.27	0.090	0.092
NGC4649	1994/01/07	5	F	4/2	38.8	38.8	38.8	38.8	0.18	0.11	0.070	0.072
NGC499	1994/01/23	1.4	F	2	28.0	28.1	38.9	38.8	0.031	0.031	5.1e-3	8.8e-3
NGC507	1994/01/23	1.4	F	2	28.0	28.1	38.9	38.8	0.052	0.039	0.020	0.016
NGC720	1993/07/17	3.3	B	4	34.9	35.0	36.3	36.3	0.033	0.026	8.7e-3	0.011
NGC4374	1993/07/04	5	B	4/2	19.3	19.4	20.5	20.5	0.048	0.088	0.020	0.037
IC4296	1994/02/15	1.8	F	2	35.8	35.8	37.1	37.1	0.025	0.018	8.5e-3	0.010
NGC4382	1994/05/27	5	F	2/1	33.1	33.4	35.3	35.3	0.045	0.035	0.011	0.013
IC1459	1993/05/20	3	B	4	19.5	19.5	19.3	19.3	0.043	0.032	0.016	0.018
NGC4365	1993/06/28	5	B	4	35.7	35.7	36.5	36.5	0.019	0.019	0.013	0.015

^aSIS data mode. F: Faint mode, B: Bright mode, 4: 4 CCD mode, 2: 2 CCD mode, 1: 1 CCD mode

^bBackground subtracted value

Table 3. The Best-fit parameters and 90% confidence errors from the RS model fitting

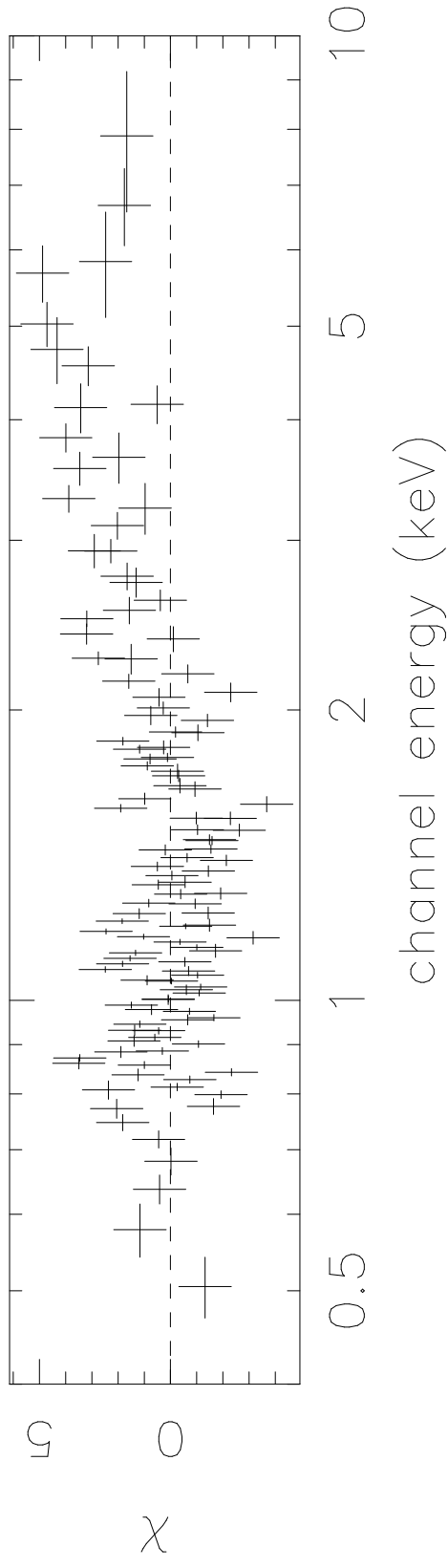
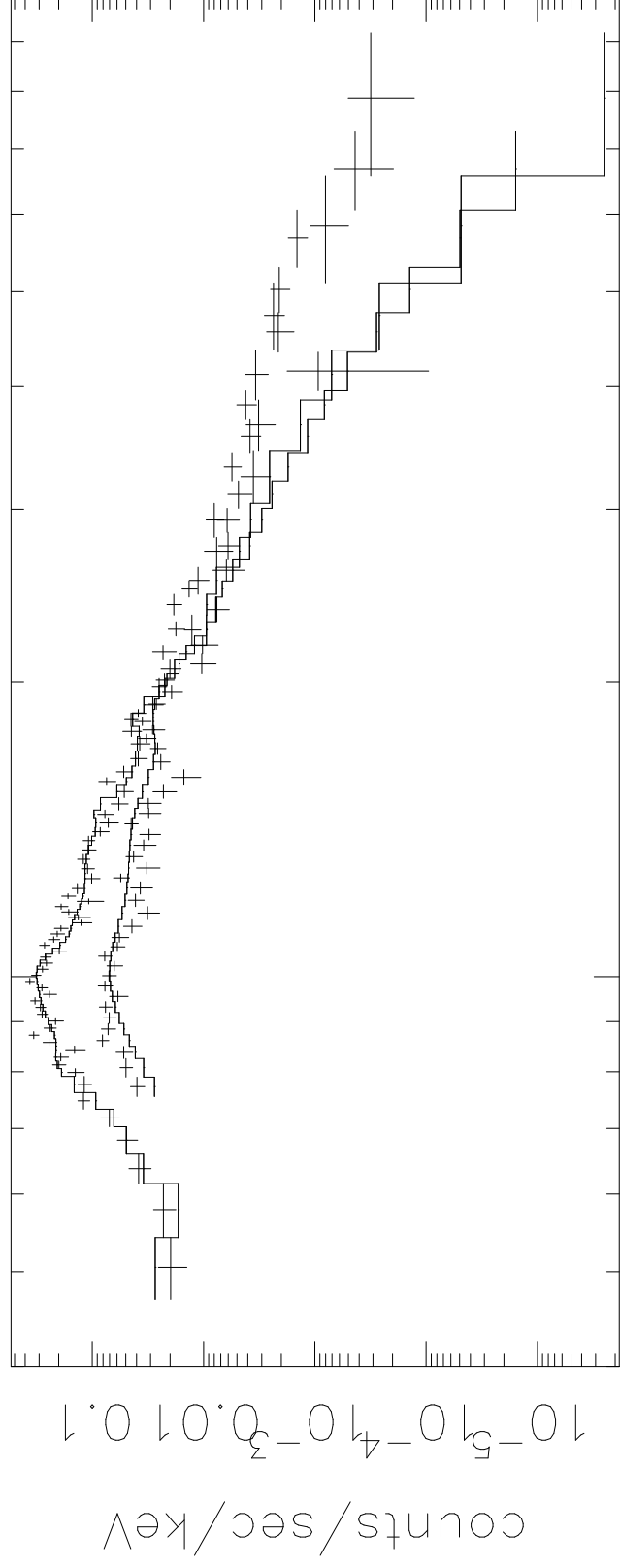
Target	N_H	kT	Abundance ^a	VEM^b	F_X in 0.5 – 4.5 keV		L_X in 0.5 – 4.5 keV		$\chi^2/d.o.f.$
	(10^{20}cm^{-2})	(keV)	(solar)	(10^{64}cm^{-3})	soft comp. (erg/sec)	hard comp. (erg/sec)	soft comp. (erg/sec)	hard comp. (erg/sec)	
NGC4472	13.4 (11.3–15.5)	0.89 (0.88–0.90)	0.39 (0.33–0.45)	5.9 (5.2–6.7)	5.5e-12	9.0e-13	6.2e41	8.4e40	442.1/425
NGC4406	10.9 (8.5–13.0)	0.84 (0.83–0.86)	0.31 (0.26–0.38)	6.3 (5.2–7.3)	5.6e-12	4.2e-13	6.0e41	3.9e40	708.3/616
NGC4636	4.9 (3.6–6.3)	0.76 (0.75–0.77)	0.31 (0.28–0.35)	5.0 (4.4–5.6)	5.9e-12	3.9e-13	5.4e41	3.3e40	732.9/428
NGC4649	16.1 (13.0–19.7)	0.85 (0.83–0.86)	0.34 (0.28–0.44)	2.7 (2.2–3.3)	2.3e-12	7.1e-13	2.8e41	6.8e40	605.7/545
NGC499	7.8 (1.0–16.1)	0.71 (0.67–0.76)	0.25 (0.18–0.47)	21.3 (12.8–26.6)	1.5e-12	<1.2e-13	2.0e42	<1.4e41	123.0/115
NGC507	10.7 (6.4–15.6)	1.01 (0.96–1.05)	0.29 (0.20–0.42)	33.0 (24.5–42.6)	1.9e-12	2.5e-13	2.6e42	3.1e41	317.0/177
NGC720	0.0 (<1.3)	0.65 (0.61–0.68)	0.098 (0.069–0.14)	1.9 (1.5–2.5)	5.5e-13	2.2e-13	1.0e41	4.1e40	150.3/139
NGC4374	12.1 (3.3–20.0)	0.67 (0.59–0.81)	0.052 (0.029–0.12)	3.5 (1.7–5.5)	1.2e-12	4.7e-13	1.4e41	4.3e40	274.9/317
IC4296	6.8 (<27.0)	0.84 (0.79–0.88)	1.1 (>0.32)	1.1 (0.18–3.7)	3.7e-13	4.5e-13	2.8e41	3.1e41	139.7/110
NGC4382	19.0 (0.43–32.5)	0.28 (0.22–0.33)	0.056 (0.029–0.21)	4.3 (0.53–18.3)	3.7e-13	5.3e-13	7.3e40	5.2e40	280.4/217
IC1459	0.0 (<4.1)	0.71 (0.64–0.79)	0.17 (>0.065)	0.64 (0.024–1.4)	2.2e-13	7.2e-13	4.8e40	1.6e41	84.11/109
NGC4365	0.0 (<32.8)	0.56 (0.22–0.72)	0.12 (>0.016)	0.11 (0.0022–8.7)	8.4e-14	3.9e-13	6.6e39	3.1e40	200.2/218

^aWe assumed the solar ratio of number density of iron to that of hydrogen is 4.68×10^{-5} (Anders and Grevesse 1989)

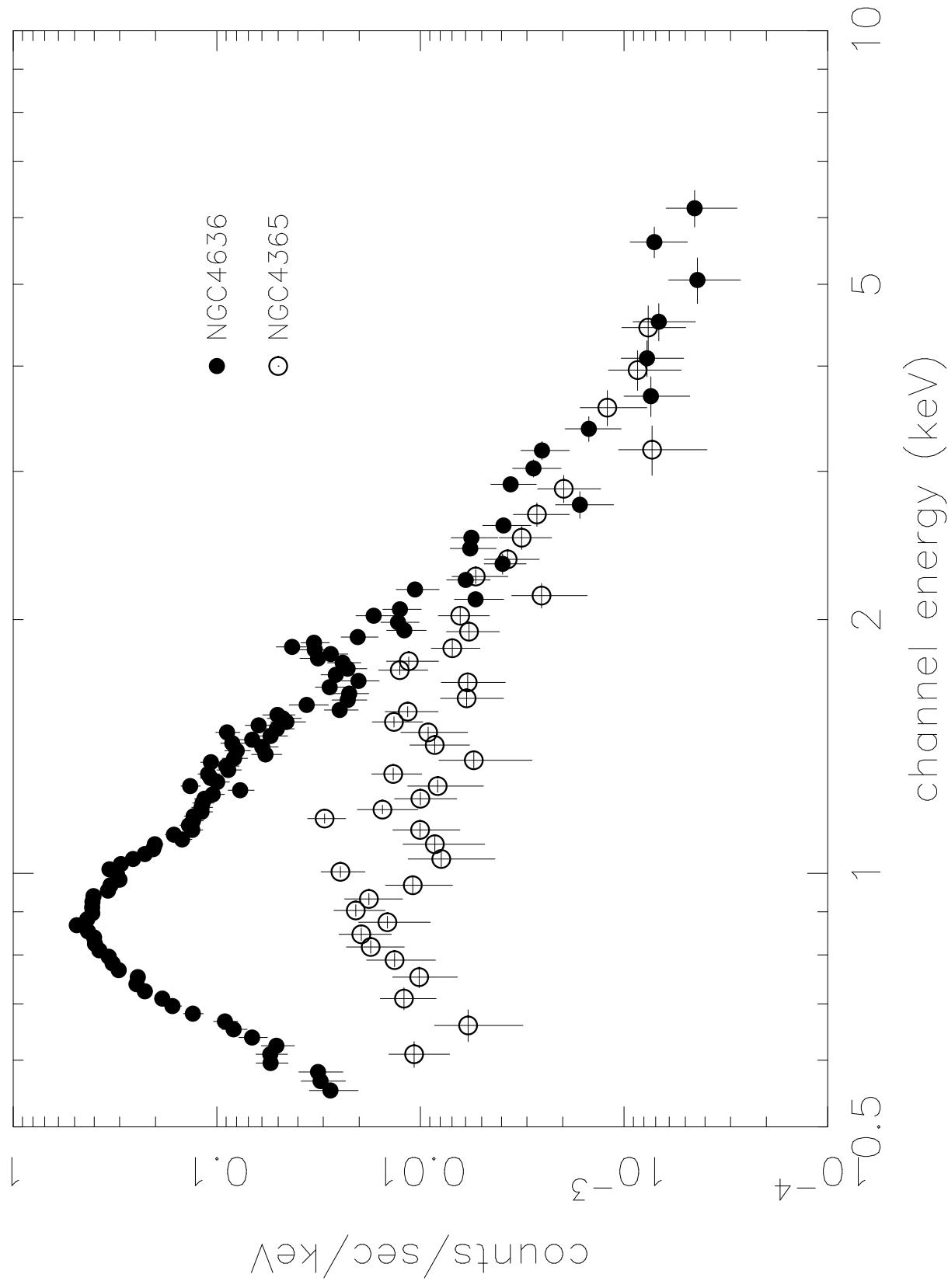
^bVolume Emission Measure of the soft component

single-temperature model

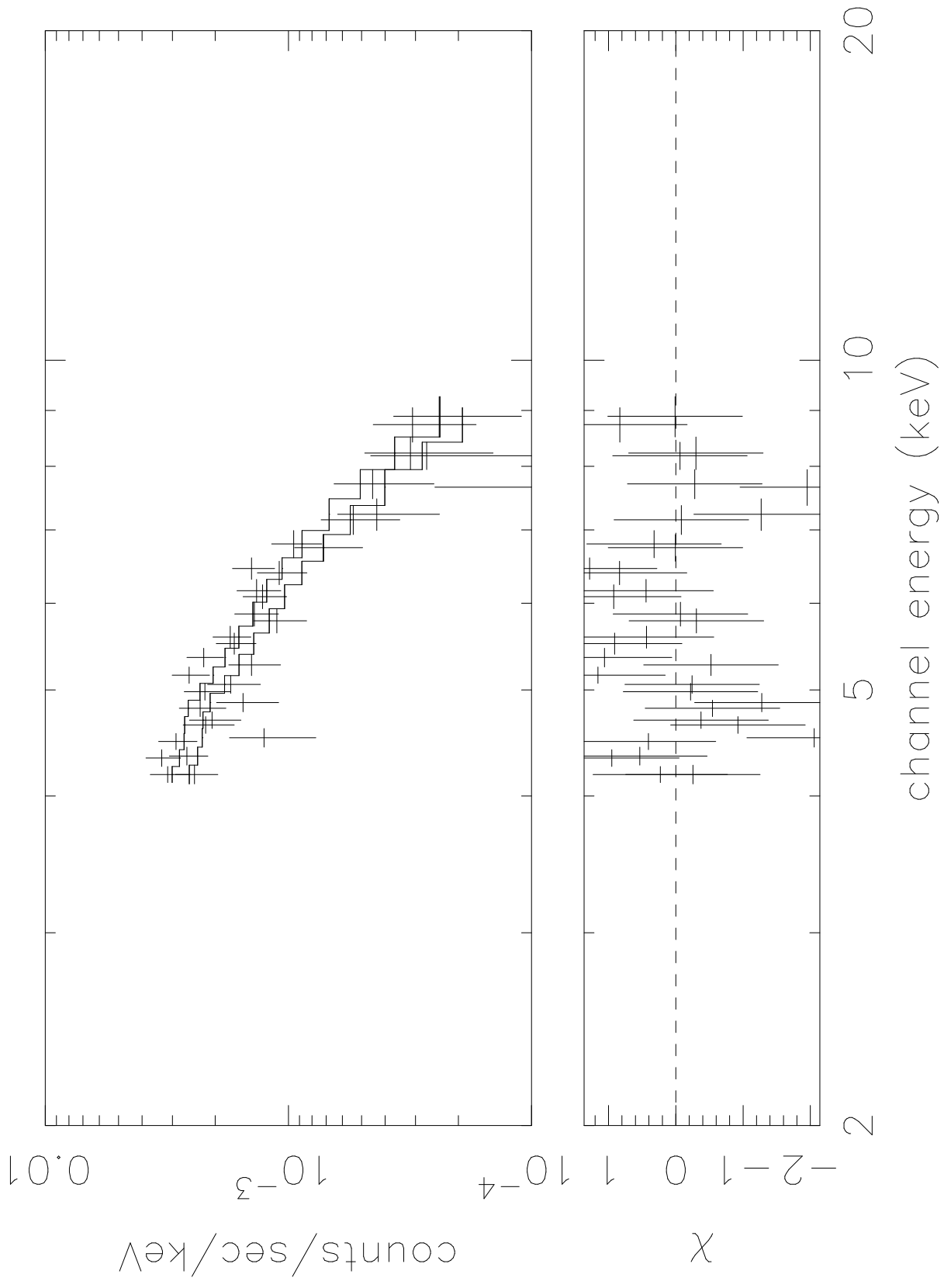
NGC4649 SISO, GIS2



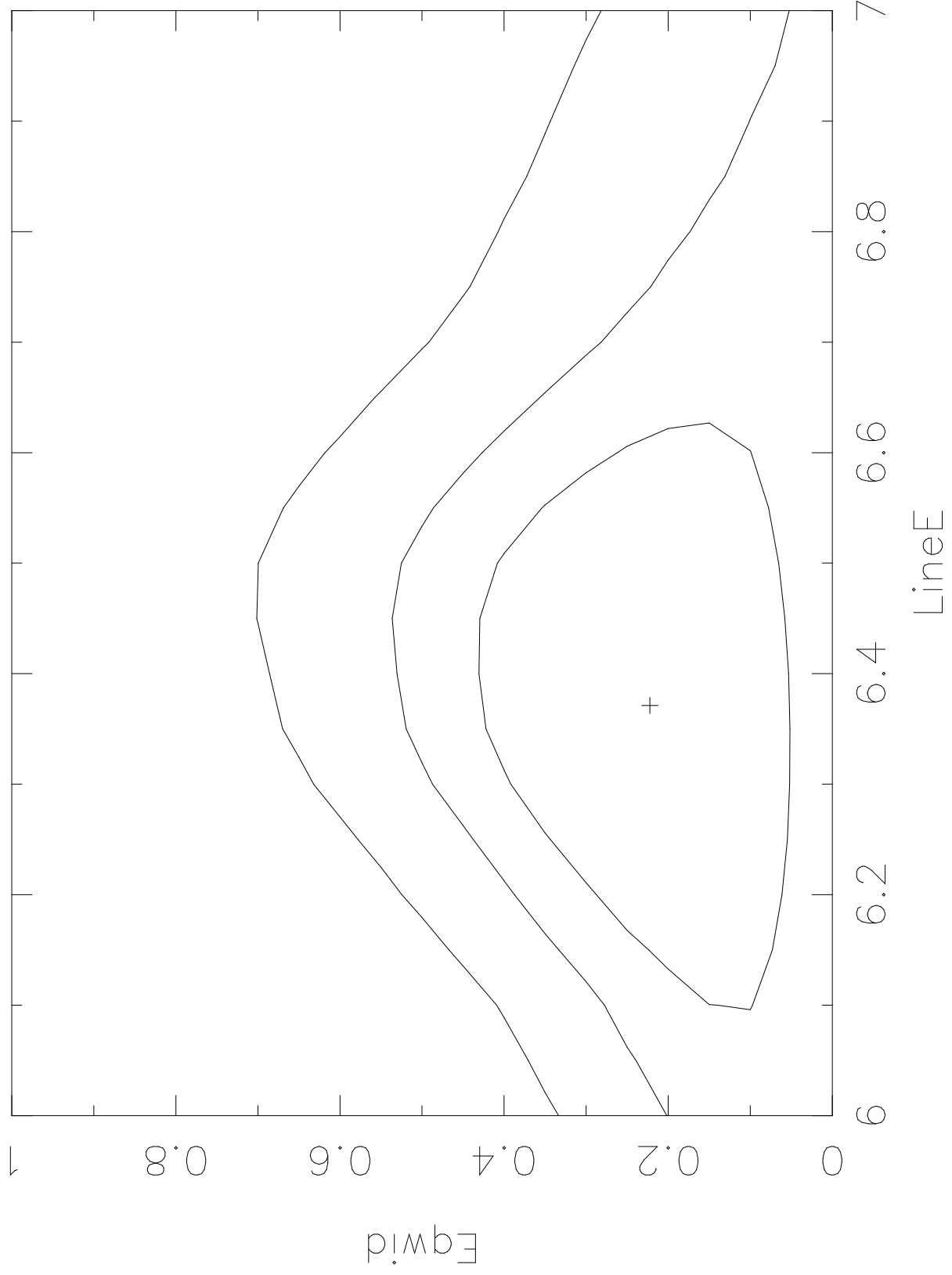
The SIS0 spectra of NGC4636 and NGC4365



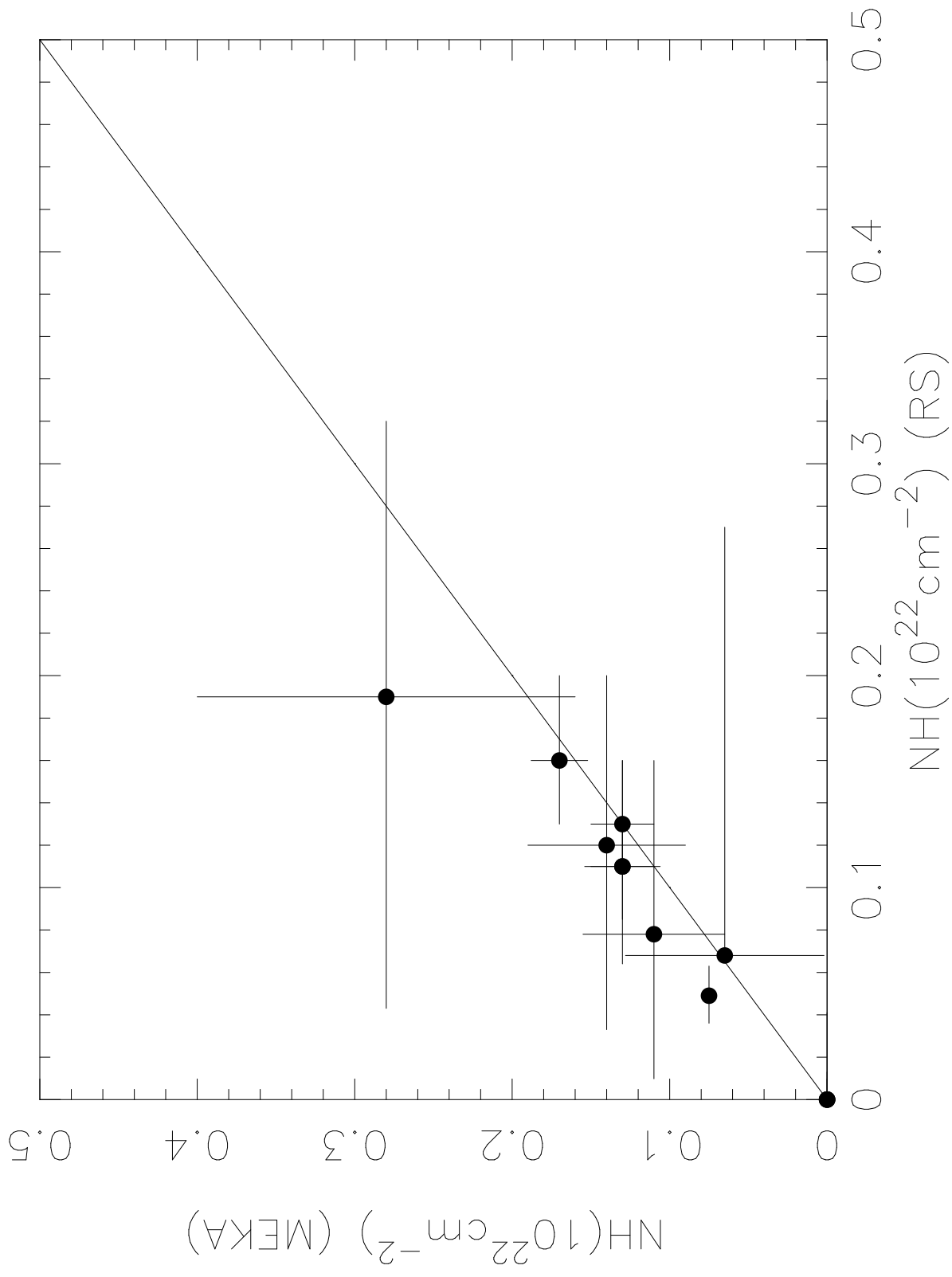
GIS composite spectra

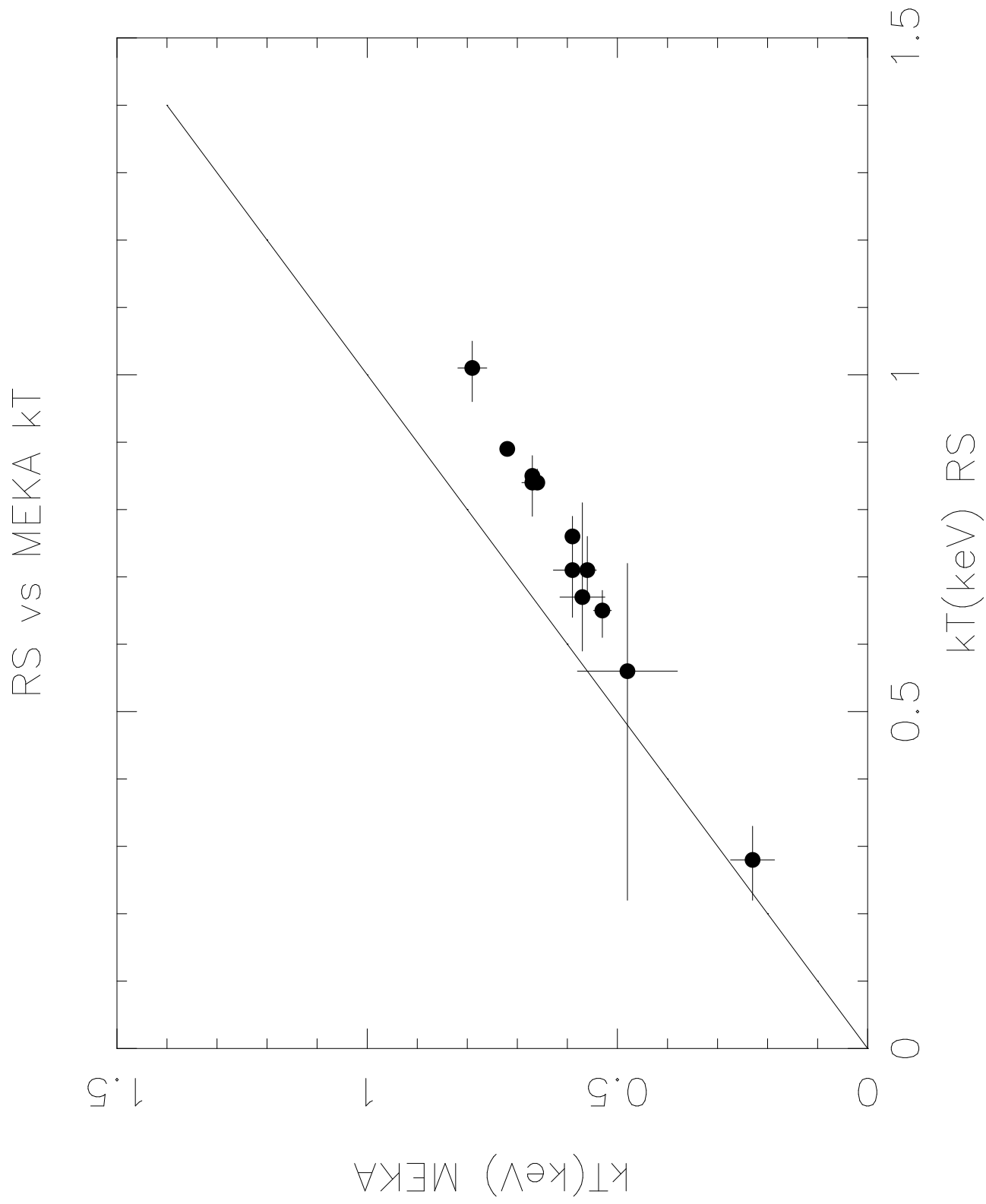


Confidence contours

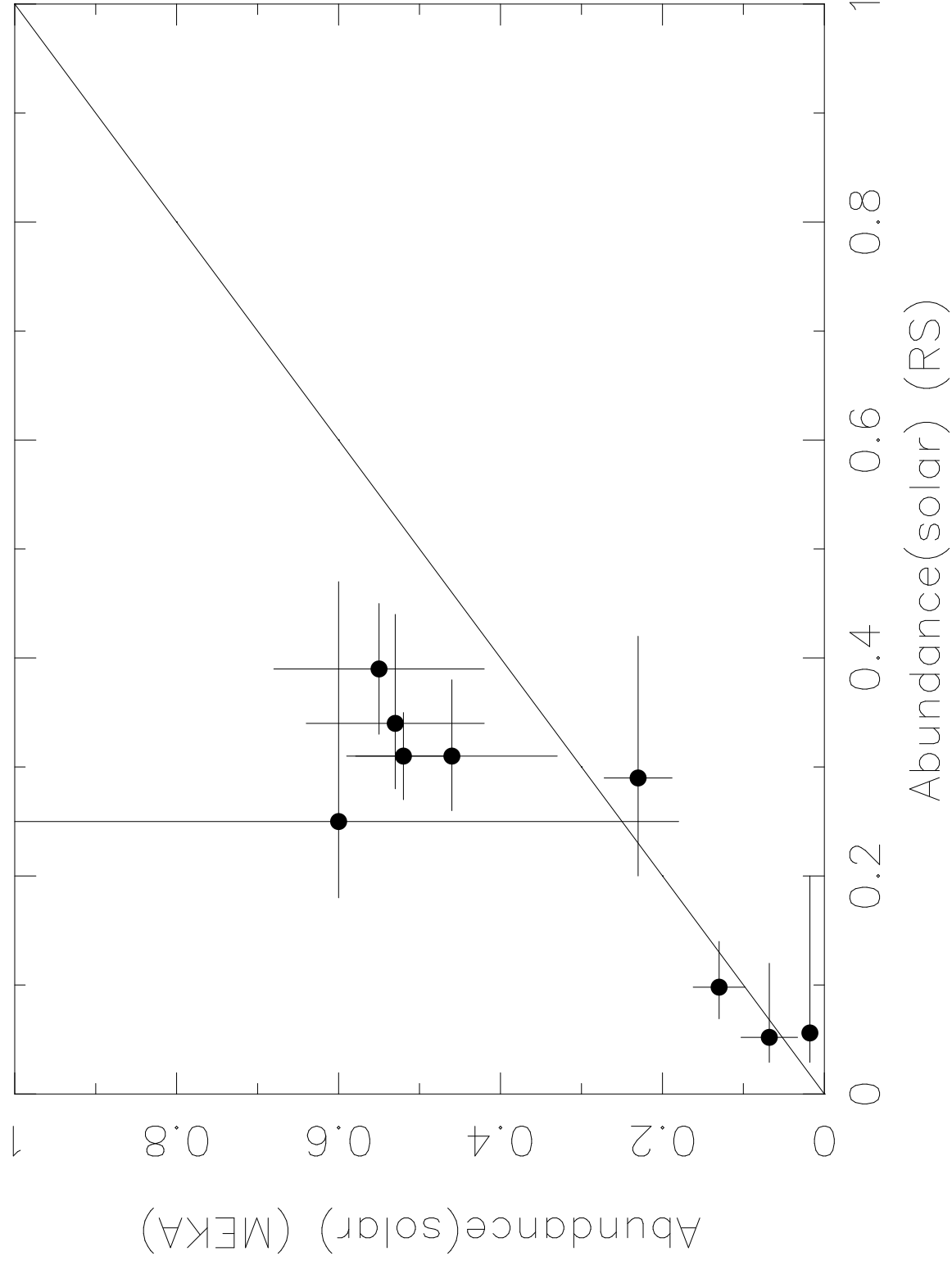


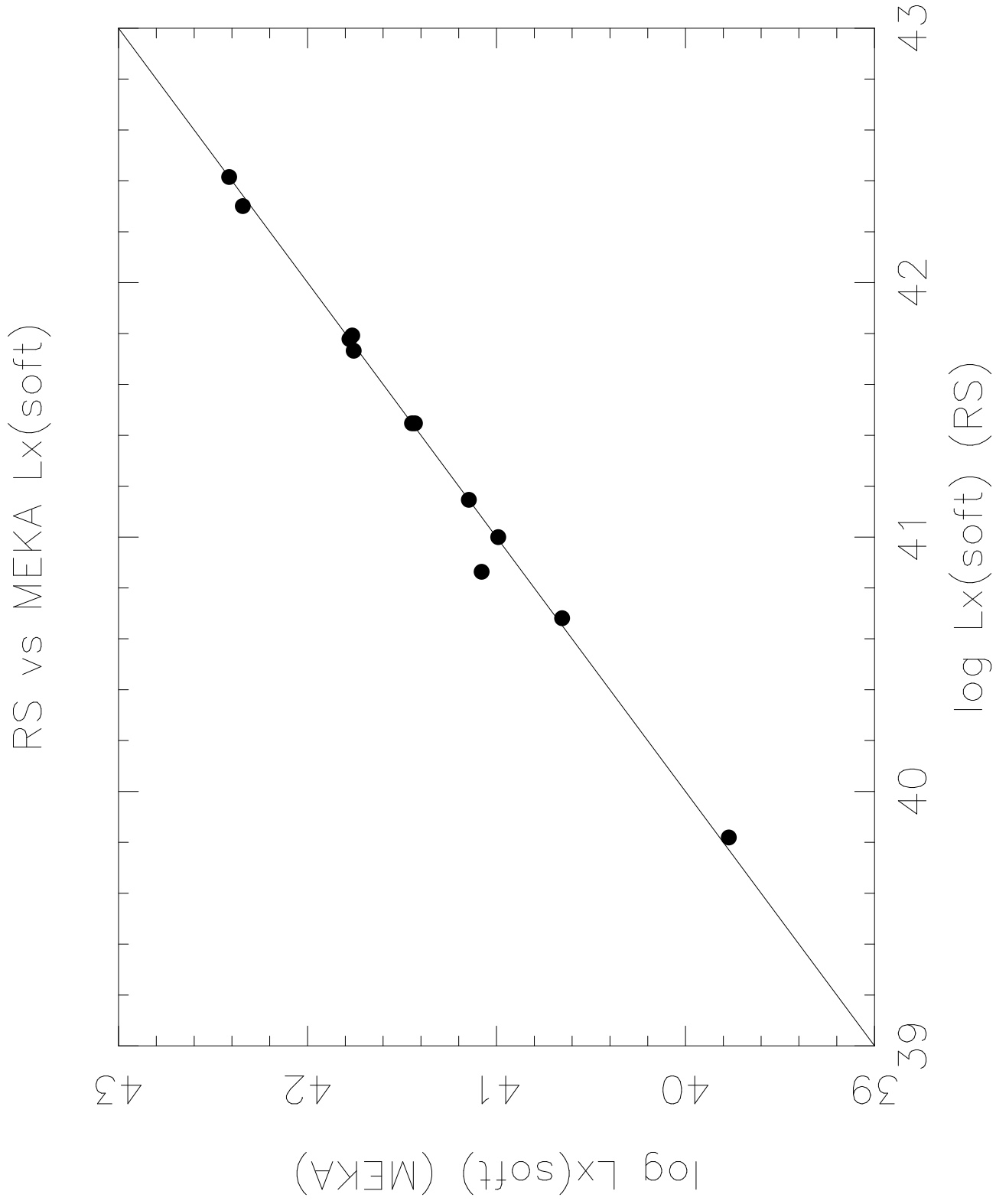
RS vs MEKA NH

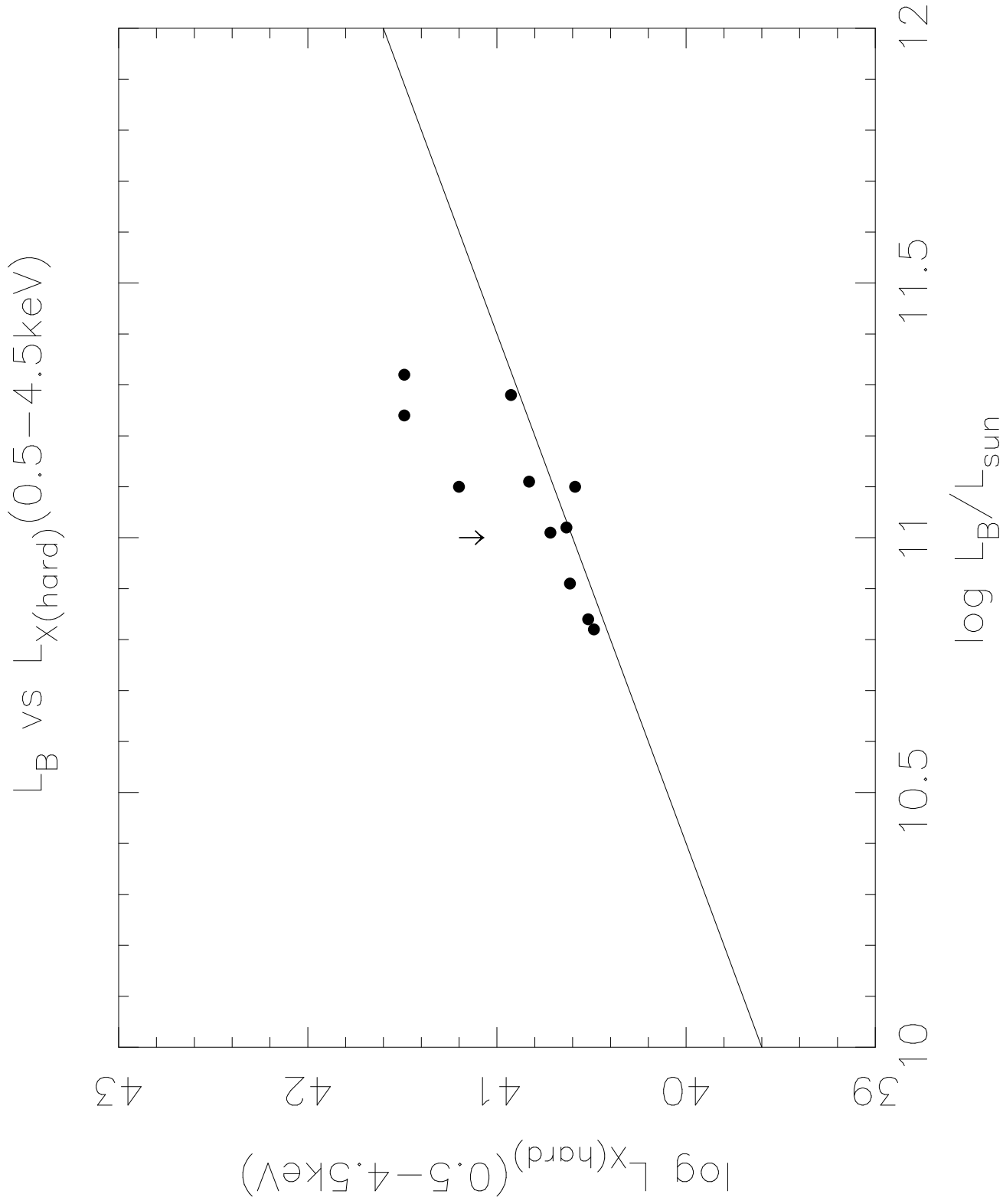


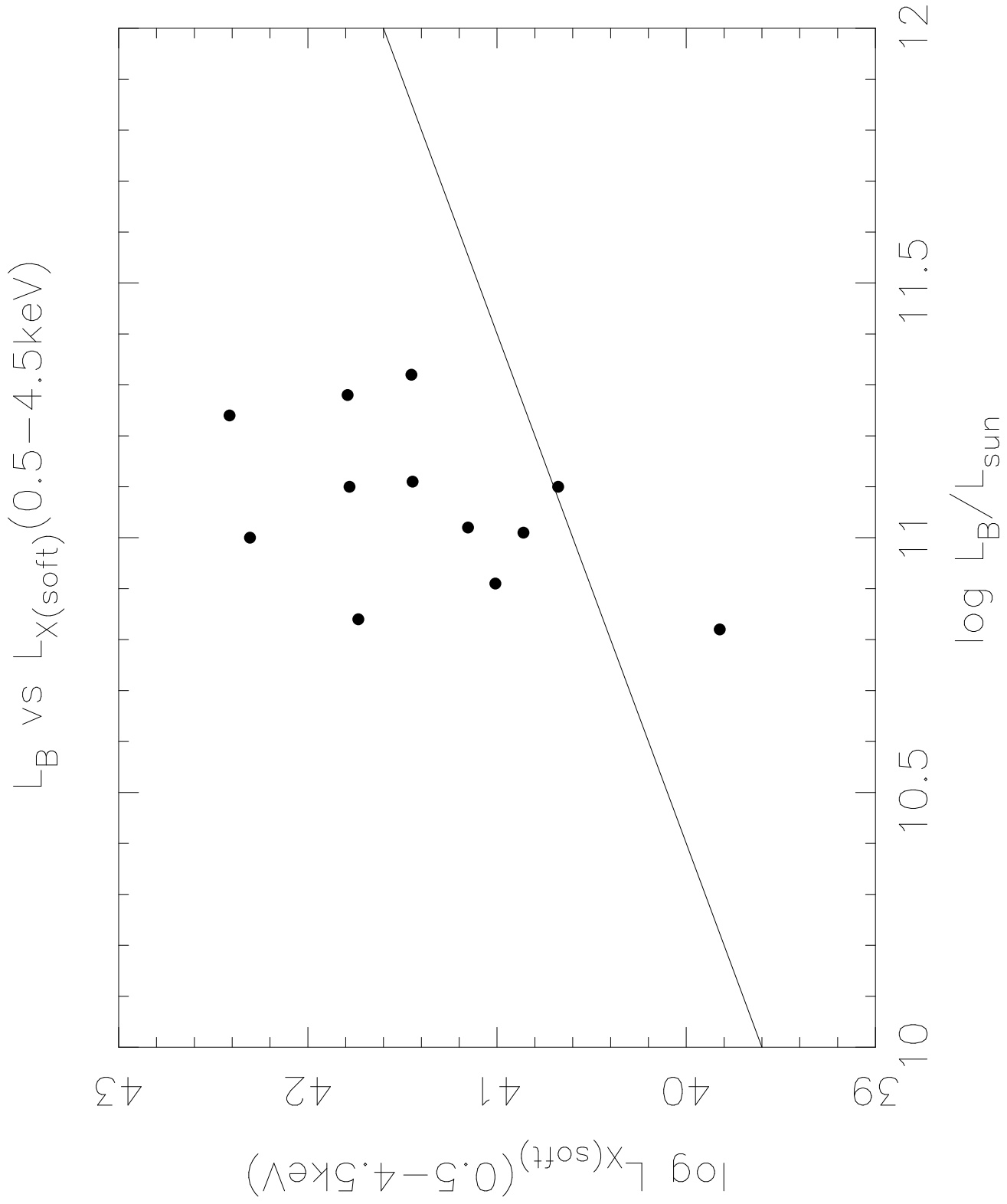


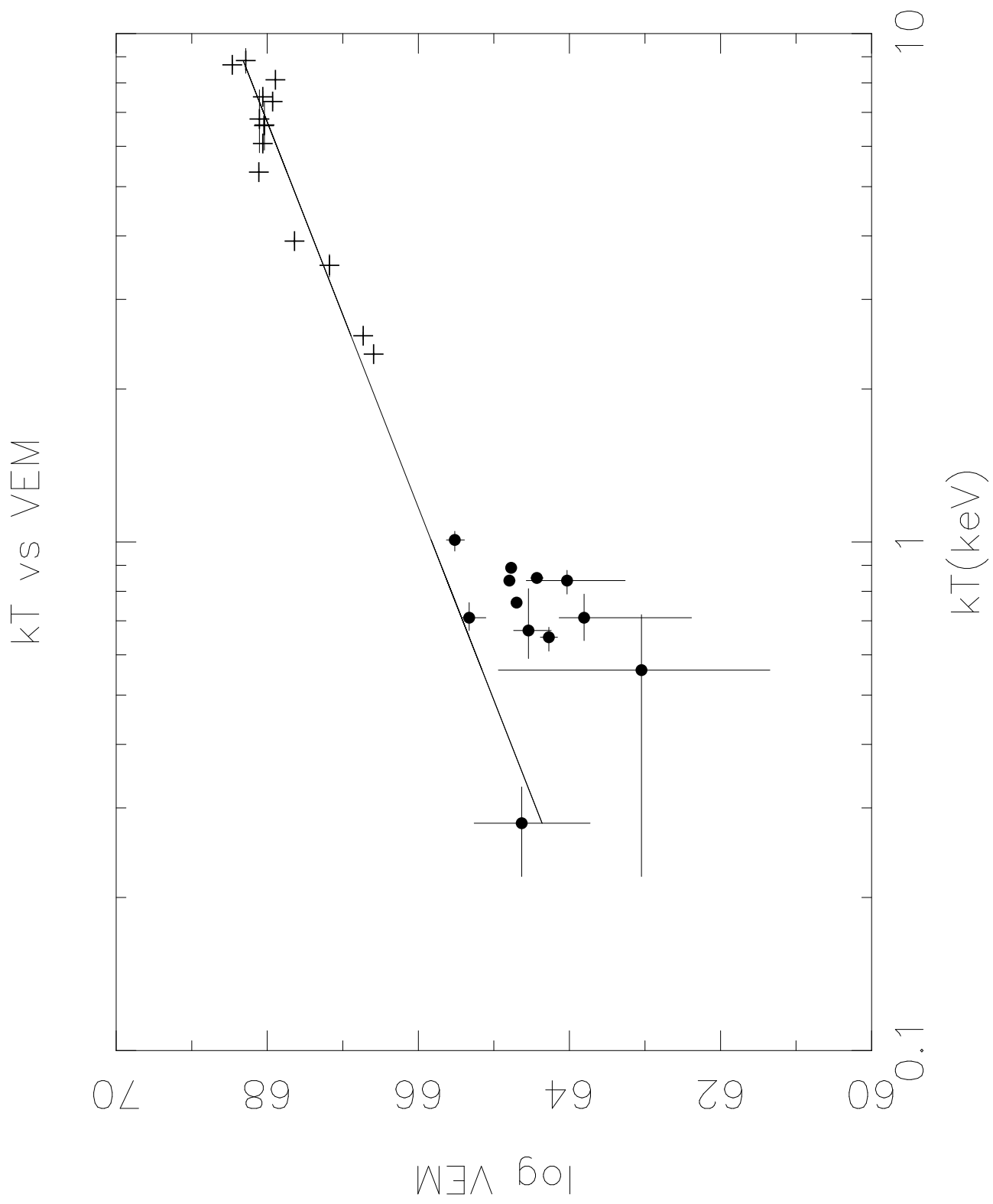
RS vs MEKA Abundance











P1 = 2.639 , P2 = 65.82

